Correlation between charge density waves and antiferromagnetism in $Nd_{1-x}Gd_xNiC_2$ solid solutions

Marta Roman,* Tomasz Klimczuk, and Kamil K. Kolincio†
Faculty of Applied Physics and Mathematics, Gdansk University of Technology, Narutowicza 11/12, PL-80-233 Gdansk, Poland

(Received 23 April 2018; revised manuscript received 15 June 2018; published 23 July 2018)

We report a study on the evolution of a charge density wave and antiferromagnetism in the series of the polycrystalline solid solution $Nd_{1-x}Gd_xNiC_2$ ($0 \leqslant x \leqslant 1$) by means of magnetic and transport properties measurements. The experimental results reveal the violation of the de Gennes law and a strong correlation between the Peierls, Néel, and Curie-Weiss temperatures, which strongly suggests a cooperative interaction between the charge density wave state and antiferromagnetism due to Fermi surface nesting enhancement of the Ruderman-Kittel-Kasuya-Yosida interaction. We also find that the obtained results for the $Nd_{1-x}Gd_xNiC_2$ ($0 \leqslant x \leqslant 1$) series overlap with the T_{CDW} trend line in the phase diagram for $RNiC_2$ family.

DOI: 10.1103/PhysRevB.98.035136

I. INTRODUCTION

Quasi-low-dimensional systems offer a large variety of unique physical properties such as charge density wave (CDW) or spin density wave (SDW) instabilities [1–3]. The low dimensionality of the electronic structure is also seen as an important ingredient of high temperature superconductivity (SC) and the charge density wave state has been found to be a universal feature in the phase diagrams of the cuprate superconductor family [4–11]. For this reason, the interplay between various types of ordering such as CDW, SC, and magnetism is a central issue in solid state physics [12–20]. The rich phase diagram of the low-dimensional rare-earth nickel dicarbides $RNiC_2$ in which various ground states such as ferromagnetic (FM), antiferromagnetic (AFM), superconducting, and charge density wave states have been reported so far, makes the members of this family appropriate candidates for the investigation of the relations between numerous types of ordering. The ground state of the members of this family depends on the rare-earth metal component denoted by R. $LaNiC_2$ is a noncentrosymmetric superconductor below $T_{sc} = 2.7$ K [21–25], $SmNiC_2$ undergoes a ferromagnetic transition at $T_C = 17.5$ K [26] and the rest of the compounds (apart from $PrNiC_2$ where a weak magnetic anomaly is observed [26,27]) order antiferromagnetically [26,28,29]. In this system, the magnetic order originates entirely from the $4f$ electrons of the rare-earth ions R^{3+} acting as local magnetic moments interacting through the Ruderman-Kittel-Kasuya-Yosida (RKKY) interaction. The CDW state has been found for most of the members of the $RNiC_2$ family (R = Pr–Lu) with the temperature ranging from 89 K for $PrNiC_2$ to 463 K for $LuNiC_2$ [30–36]. Remarkably the Peierls temperature T_{CDW} has been found to scale linearly with the unit-cell for for R ranging from Sm to Lu. The linear scaling is also relevant for the lock-in transition temperature T_1 in the range from R = Gd to Ho [36]. This effect has been tentatively attributed to the evolution of the Fermi surface (FS) topology resulting in the modification of the nesting conditions. Interestingly, the Peierls temperature for Nd and Pr bearing compounds deviates from the linear trend observed for the rest of the family.

The CDW in $RNiC_2$ has been found to interact with the magnetic state. For $SmNiC_2$, the Peierls instability is completely suppressed below the Curie temperature [37–40], in contrast with $PrNiC_2$, where the magnetic anomaly has been found to have a constructive impact on the nesting properties [27,41]. In the compounds showing the antiferromagnetic ground state, a CDW partially survives below the Néel temperature [27,41–43]. Recently Hanasaki *et al.* [43] suggested that the AFM order originates from the cooperative effect involving a CDW and spin oscillations. These reports inspired us to explore the evolution of a CDW instability and magnetism on the path between $NdNiC_2$ and $GdNiC_2$, both exhibiting an antiferromagnetic ground state and standing on opposite sides of the deviation from the linearity on the $RNiC_2$ phase diagram.

In this paper we report a detailed investigation on the solid solution $Nd_{1-x}Gd_xNiC_2$ ($0 \leqslant x \leqslant 1$) by means of powder x-ray diffraction, ac and dc magnetic susceptibility and electrical resistivity. The results were discussed with a particular emphasis on the interrelationship between a CDW state and antiferromagnetic ordering.

II. EXPERIMENTAL

The series of the polycrystalline $Nd_{1-x}Gd_xNiC_2$ solid solutions for Gd concentration $0 \leqslant x \leqslant 1$ were prepared by arc melting of the proper amounts of pure elements: Ni (3N), C (5N), Nd (3N), and Gd (3N) in a high purity argon atmosphere with a zirconium button used as an oxygen getter. To compensate for the loss during the arc-melting process additional amounts of rare-earth metals (≈2%) and carbon (≈3%) were used. All samples were turned over and remelted four times on a water-cooled copper hearth in order to obtain good homogeneity. All the samples obtained from arc melting were wrapped in tantalum foil, placed in an evacuated quartz tube, annealed at 900 °C for 12 days and cooled down to room temperature by quenching in cold water.

*mroman@mif.pg.gda.pl
†kamkolin@pg.edu.pl

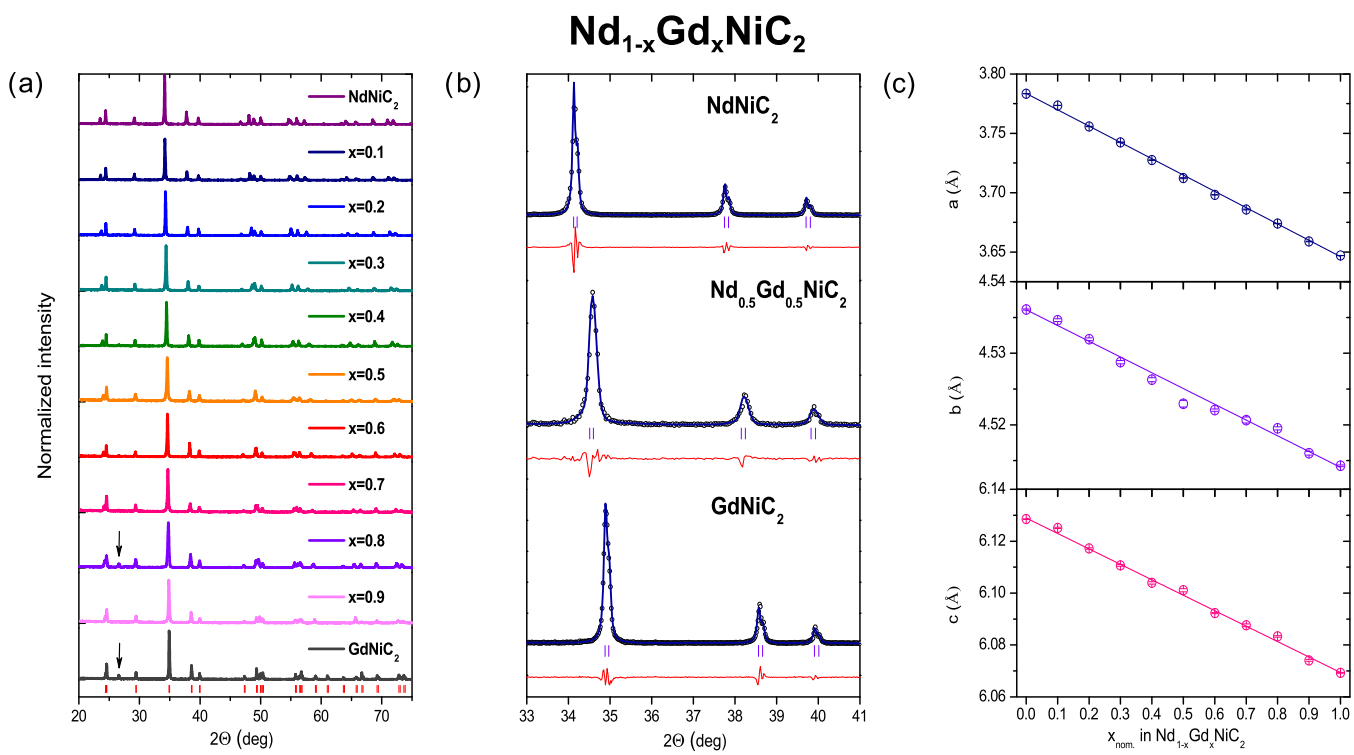

FIG. 1. (a) Powder x-ray diffraction (pXRD) patterns for the series $Nd_{1-x}Gd_xNiC_2$ ($0 \leqslant x \leqslant 1$). The vertical ticks correspond to the Bragg peaks for $Nd_{1-x}Gd_xNiC_2$. Arrows indicate the peaks corresponding to residual carbon content. (b) Expanded view of the main reflection line (111) showing a shift towards higher angles by substituting Nd for Gd. Open circles denote experimental points, whereas calculated diffraction patterns are represented by the solid blue lines. Differences between experiment and a model are shown by the red lines. (c) Change of a, b, and c lattice parameters for the series $Nd_{1-x}Gd_xNiC_2$ ($0 \leqslant x \leqslant 1$).

Overall loss of weight after the melting and annealing process was negligible ($\leqslant$1%) indicating that the elemental concentration was close to the actual alloying level.

For the crystal structure determination, powder x-ray diffraction (pXRD) measurements were performed using a X'Pert PRO-MPD, PANalitycal diffractometer with Cu K_α radiation, in the 2θ range from 20° to 75°. The lattice parameters were determined from a LeBail profile refinement of x-ray diffraction patterns for the entire $Nd_{1-x}Gd_xNiC_2$ series executed using FULLPROF software [44].

The physical property measurements were performed in the temperature range of 1.9–300 K by using a commercial Physical Property Measurement System (Quantum Design). Magnetization measurements were carried out using the ac and the dc Susceptibility Option (ACMS). A standard four-probe contact configuration was used to measure the electrical resistivity and the platinum wires ($\phi = 37\mu$m) were attached to the polished samples by spot welding.

III. RESULTS AND DISCUSSION

The phase composition and crystallographic structure of the obtained samples were checked at room temperature by powder x-ray diffraction which revealed that all observed reflections for the $Nd_{1-x}Gd_xNiC_2$ ($0 \leqslant x \leqslant 1$) series are indexed in the orthorhombic $CeNiC_2$-type structure with the space group $Amm2$. The pXRD patterns for $Nd_{1-x}Gd_xNiC_2$ solid solutions are presented in Fig. 1(a). Only for the $x = 0.8$ and $x = 1$ samples, additional weak reflection lines (marked by arrows) corresponding to residual carbon content are observed. The substitution of Nd with Gd does not change the crystal structure symmetry. However, one can observe that the Bragg reflection lines are shifted towards higher angles with an increase in the Gd content [shown in Fig. 1(b)]. This behavior is consistent with Gd^{3+} having a smaller ionic radius than Nd^{3+} and confirms successful chemical alloying.

The unit cell parameters determined from LeBail refinement for the parent compounds $NdNiC_2$ and $GdNiC_2$ were found to be $a = 3.783(1)$ Å, $b = 4.536(1)$ Å, $c = 6.129(1)$ Å, and $a = 3.647(1)$ Å, $b = 4.514(1)$ Å, $c = 6.069(1)$ Å, respectively. These values are in good agreement with those reported in the literature [45]. The refined lattice parameters for the intermediate samples from the $Nd_{1-x}Gd_xNiC_2$ series are shown in Fig. 1(c). The a, b, and c parameters decrease linearly with an increase in the Gd concentration for the whole x range, and hence obey Vegard's law. The a constant expands by almost 4% whereas the changes of the b and c parameters are less pronounced (below 1%). The smallest change is observed for the b parameter, which could be associated with the rigid C-C dimers along the b axis [30].

The electrical resistivity for the $Nd_{1-x}Gd_xNiC_2$ ($0 \leqslant x \leqslant 1$) series was measured without an applied magnetic field in the temperature range 1.9–250 K and the results (ρ/ρ_{250K} vs T) are shown in Fig. 2. The whole series exhibits typical metallic behavior at high temperatures showing a decrease of the electrical resistivity with decreasing temperature. With further cooling, a minimum followed by a hump well known to be a characteristic feature of a charge density wave transition, is observed for the

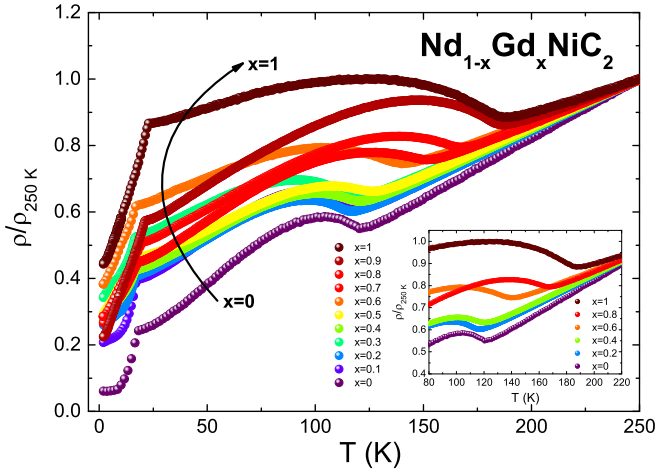

FIG. 2. Temperature dependence of the normalized electrical resistivity ρ/ρ_{250K} (T) for $Nd_{1-x}Gd_xNiC_2$ $(0 \leqslant x \leqslant 1)$. Inset shows the vicinity of the CDW transition for selected samples for better clarity.

entire concentration of Gd in the $Nd_{1-x}Gd_xNiC_2$ series. The temperature of the CDW formation (T_{CDW}) was obtained from the temperature derivative of the resistivity ($d\rho/dT$) and for the parent compounds $NdNiC_2$ and $GdNiC_2$, T_{CDW} is 130 K and 197 K, respectively. The inset of Fig. 2. shows the expanded view of the normalized electrical resistivity in the vicinity of the CDW transition for selected $Nd_{1-x}Gd_xNiC_2$ samples. With the increase in the Gd concentration, the temperature of the CDW transition (T_{CDW}) for the $Nd_{1-x}Gd_xNiC_2$ series starts to decrease from 130 K for $x = 0$ (purple spheres), reaching a minimum of 123 K for the Gd concentration $x = 0.2$ (blue spheres) and then increases more rapidly with a further increase of Gd up to 197 K for $x = 1$ (brown spheres). Upon further cooling, the electrical resistivity for the whole series continues to decrease until the visible drop in resistivity at low temperatures. For $GdNiC_2$ and $NdNiC_2$ this effect has been reported to be caused by an antiferromagnetic transition, and therefore it is reasonable to expect the same behavior for the intermediate compounds [41,46].

The temperature dependence of the magnetic susceptibility $\chi(T)$ for the $Nd_{1-x}Gd_xNiC_2$ $(0 \leqslant x \leqslant 1)$ series measured with a $\mu_0 H = 1\,T$ applied magnetic field is depicted in Fig. 3(a) (shown only for selected samples for better clarity). At high temperatures the entire series shows paramagnetic behavior. Between 16 K and 22 K (depending on x), $\chi(T)$ reveals a sharp maximum. The Néel temperature (T_N) was estimated as the maximum of the temperature derivative of the magnetic susceptibility multiplied by the temperature ($d(\chi T)/dT$). The obtained T_N values are in good agreement with those determined from the resistivity measurement. An additional minimum followed by a further increase is observed for most members from the $Nd_{1-x}Gd_xNiC_2$ series and can be attributed to a spin-flop transition as reported for the $GdNiC_2$ compound [43,47].

Above T_N, the entire series obeys the Curie-Weiss law. The $\chi(T)$ were fitted using the Curie-Weiss law expression:

$$\chi(T) = \frac{C}{T - \theta_{CW}} + \chi_0, \tag{1}$$

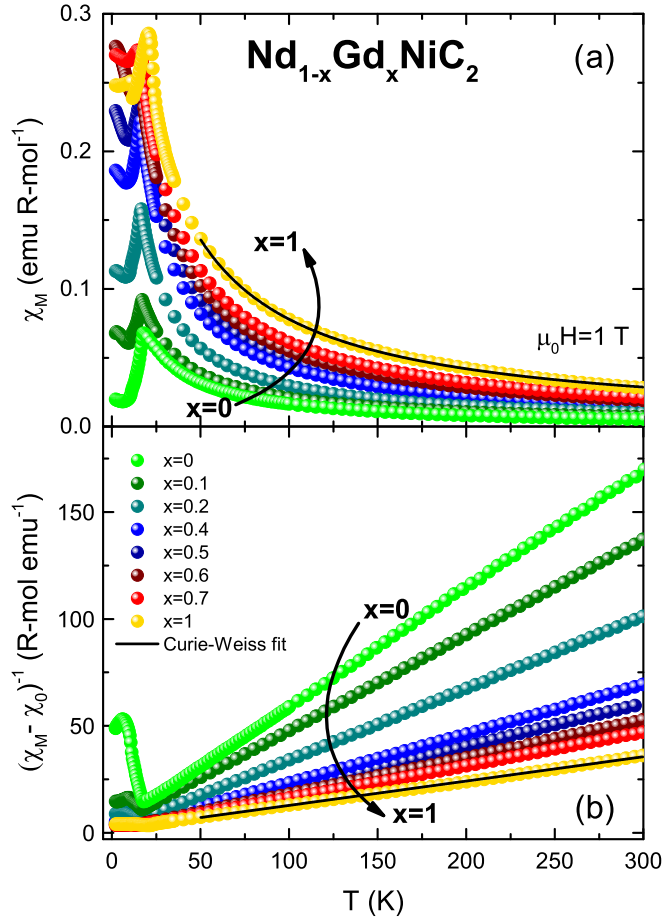

FIG. 3. Temperature dependence of the molar magnetic susceptibility χ_M (a) and of the reciprocal molar magnetic susceptibility $(\chi_M\text{-}\chi_0)^{-1}$ (b) for selected samples from the $Nd_{1-x}Gd_xNiC_2$ $(0 \leqslant x \leqslant 1)$ series.

where C is the Curie constant, θ_{CW} is the Curie-Weiss temperature, and χ_0 is the temperature-independent magnetic susceptibility which is related both to the sample and the sample holder (a small diamagnetic contribution from sample straw). An exemplary fit to the data is shown with a solid line in Fig. 3. The results of the magnetic susceptibility with a clear magnetic anomaly at T_N were also presented as a function of the reciprocal magnetic susceptibility with temperature $(\chi_M\text{-}\chi_0)^{-1}$ vs T in Fig. 3(b). Above the AFM transition temperature, all $(\chi_M\text{-}\chi_0)^{-1}$ plots show an approximate linear dependence.

Having determined the value of the Curie constant C from the Curie-Weiss fit, the effective magnetic moment μ_{eff} was calculated for each compound of the $Nd_{1-x}Gd_xNiC_2$ series using the formula,

$$\mu_{eff} = \sqrt{\frac{3Ck_B}{{\mu_B}^2 N_A}}, \tag{2}$$

where k_B is the Boltzmann constant, N_A is the Avogadro number, and μ_B is the Bohr magneton.

The Curie-Weiss temperature and the effective magnetic moment versus Gd concentration [$\theta_{CW}(x)$ and $\mu_{eff}(x)$] are presented in Figs. 4(a) and 4(b), respectively. Estimated θ_{CW} for $GdNiC_2$ denotes −18.85 K and stands in good agreement

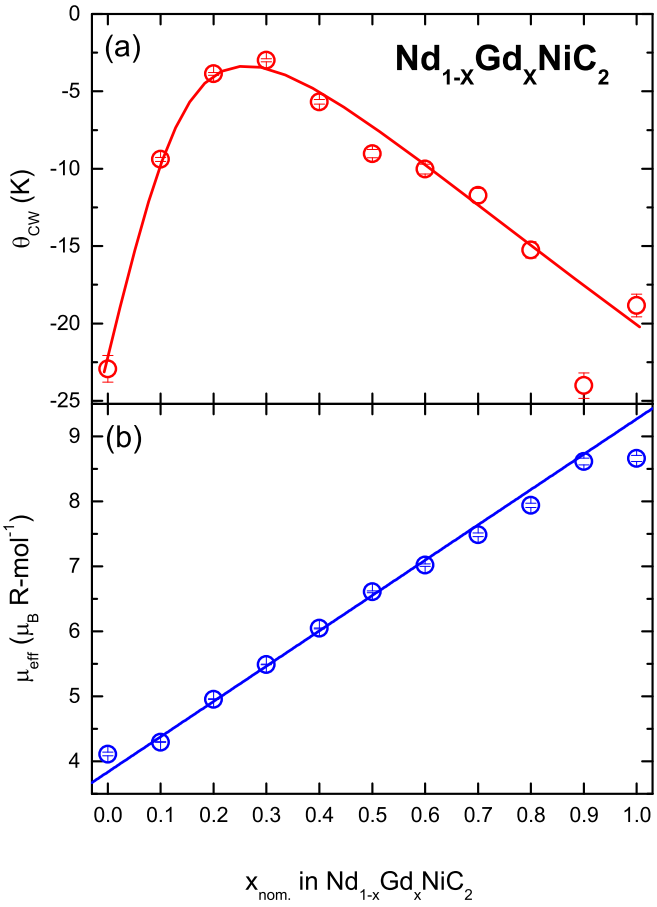

FIG. 4. Change of the Curie-Weiss temperature $\theta_{CW}(x)$ (a) and effective magnetic moment $\mu_{eff}(x)$ (b) for $Nd_{1-x}Gd_xNiC_2$ ($0 \leqslant x \leqslant 1$). Solid lines are a guide for the eye.

with previously reported values [48]. The $\theta_{CW} = -22.93$ K obtained for $NdNiC_2$ is, however, visibly different from the value reported by us previously (−5.9 K) [27]. The θ_{CW} in this compound has been found very sensitive to the direction of magnetic field and varies from −17.8 K along the b axis to 24.6 along the a axis [26]. The inconsistency with our last results can then be attributed to a difference in the sample microstructure. The negative sign of the Curie-Weiss temperature indicates antiferromagnetic fluctuations. Upon the crossover from $NdNiC_2$ to $GdNiC_2$, the θ_{CW} initially shifts towards less negative values and reaches a maximum for the intermediate compound $Nd_{0.7}Gd_{0.3}NiC_2$ ($\theta_{CW} = -1.35$ K). The proximity to zero suggests the weakness of the magnetic interactions between magnetic ions. With a further increase of the Gd concentration, θ_{CW} becomes more negative again, which is a signature of the enhancement of antiferromagnetic interactions. For $x = 0.9$, a deviation from the curve is observed and the origin of this anomaly is unknown.

In the $RNiC_2$ family, nickel atoms do not contribute to the magnetic moment and the magnetic ordering originates only from the $4f$ electrons of rare-earth ions R^{3+}. The effective magnetic moments of the parent compounds determined from the Curie-Weiss fit, ($\mu_{eff} = 4.11\mu_B$ and $8.66\mu_B$ for $NdNiC_2$ and $GdNiC_2$, respectively) are larger than the values expected for free R^{3+} ions ($3.62\mu_B$ for Nd^{3+} and $7.94\mu_B$ for Gd^{3+}) but

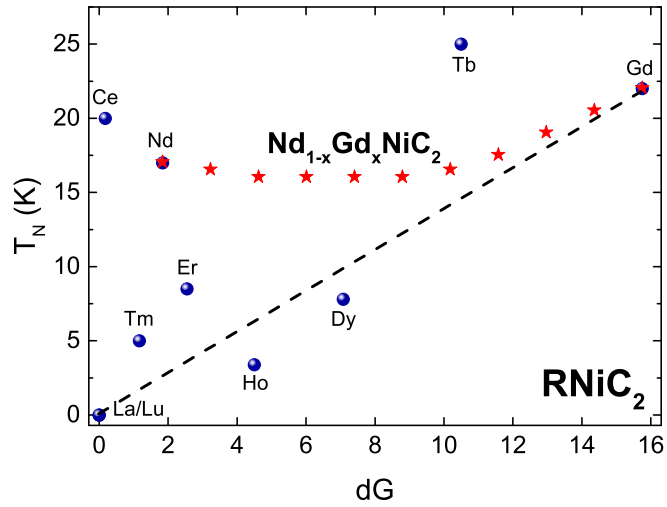

FIG. 5. The Néel temperature as a function of the de Gennes factor for the $RNiC_2$ family, including the $Nd_{1-x}Gd_xNiC_2$ solid solution.

close to the values reported previously [48,49]. The change of the effective magnetic moment with increasing level of the Gd concentration $\mu_{eff}(x)$ could be considered as linear with a small deviation for the parent compounds ($NdNiC_2$ and $GdNiC_2$). This result is consistent with what can be expected from electron introduction when Gd ($4f^7$) replaces Nd ($4f^3$) and the deviation from linearity could be caused by a disorder effect introduced by doping.

The de Gennes law describing the strength of the indirect exchange coupling between local moments predicts that, for the systems in which the magnetic ground state originates from the RKKY interaction, the Néel temperature is expected to be related to the bulk electronic density of states at the Fermi level $N(\epsilon_F)$ with the relationship,

$$T_N \sim 8N(\epsilon_F)k_B I^2 dG, \tag{3}$$

where k_B is the Boltzmann constant and I is the exchange integral. The de Gennes factor (dG) is given by the formula,

$$dG = (g_J - 1)^2 J(J + 1), \tag{4}$$

where g_J is the Landé factor and J is the total angular momentum of the R^{3+} ion following Hund's rule in the ground state. The effective dG factor for the $Nd_{1-x}Gd_xNiC_2$ solid solutions was calculated as a weighted average of the two elemental dG factors:

$$dG_{eff} = (1 - x)dG_{Nd} + (x)dG_{Gd}. \tag{5}$$

Figure 5 depicts de Gennes scaling for the members of the $RNiC_2$ family exhibiting an AFM transition, including $Nd_{1-x}Gd_xNiC_2$ studied in this paper. A clear deviation from the expected de Gennes trend indicates that the bulk RKKY interaction is not essential to describe the magnetic transition in $Nd_{1-x}Gd_xNiC_2$ and other factors have to be considered. Previously, the breakdown of the dG scaling for $TbNiC_2$ has been explained by the influence of the crystalline electric field (CEF) [50]. This scenario could be relevant in the case of $Nd_{1-x}Gd_xNiC_2$, since the deviation from the dG scaling is visibly enhanced with an increase of the Nd content. This type of crossover can be expected based on the behavior of the parent

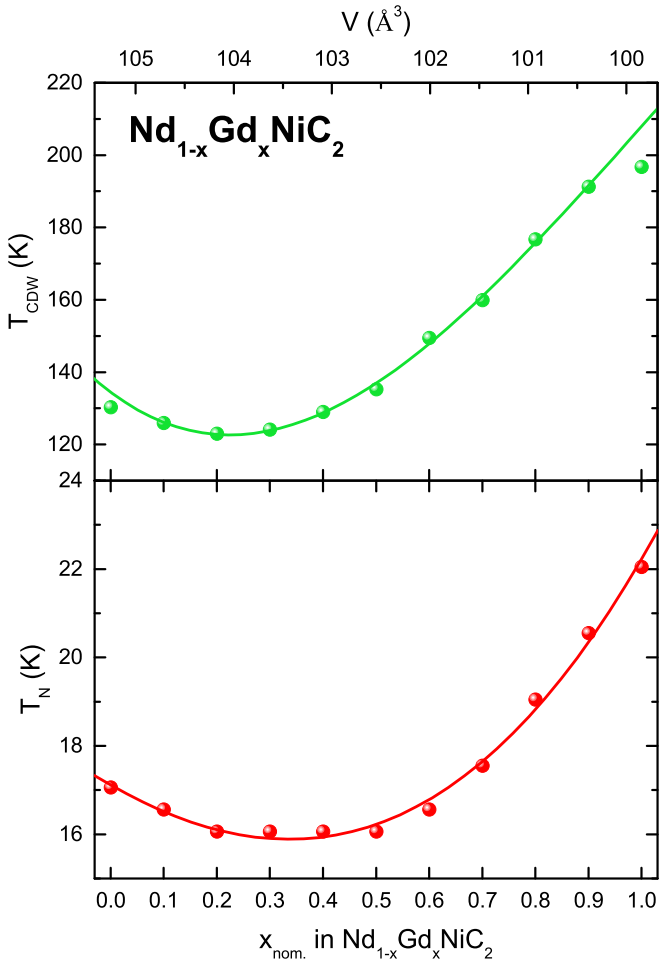

FIG. 6. Evolution of T_{CDW} (a) and T_N (b) as a function of Gd concentration $x_{nom.}$ in the $Nd_{1-x}Gd_xNiC_2$ ($0 \leqslant x \leqslant 1$).

compounds: $GdNiC_2$ shows negligible CEF [48], while the crystalline field plays a more important role in $NdNiC_2$ [26]. One must, however, find that the violation of the de Gennes law being observed for $NdNiC_2$ is notably more pronounced than the deviations from the dG scaling seen for Er and Tm bearing compounds. This observation stands in contrast with the comparison of the values of the CEF parameters A_2^0 and A_2^2 reported for these three compounds, which for $NdNiC_2$ are an order of magnitude lower than for $ErNiC_2$ and $TmNiC_2$ [26,50]. For that reason, the alternative mechanisms have to be taken into account to explain this unusual effect.

According to Eq. (4), in the discussion of T_N behavior one must also consider the role of the density of states, which is expected to be modified upon undergoing a Peierls transition inducing the opening of the electronic gap at the Fermi level and condensation of the free electronic carriers into the CDW state.

In Fig. 6 we compare the CDW transition temperature T_{CDW} [Fig. 6(a)] and the Néel temperature T_N [Fig. 6(b)] plotted against the values of the Gd concentration in the $Nd_{1-x}Gd_xNiC_2$ ($0 \leqslant x \leqslant 1$). For better clarity, the unit-cell volume is displayed above the top axis. The character of the evolution of these transition temperatures is similar and reminiscent of the behavior of $\theta_{CW}(x)$—both curves reveal the minimum with the composition corresponding to $x = 0.3$.

The correlation between the T_{CDW} and T_N suggests a strong interrelationship between the charge density wave state and antiferromagnetism. According to the de Gennes theory, one would expect a negative coupling, since the CDW transition decreases the $N(\epsilon_F)$, thus, according to Eq. (3), the CDW should have a negative impact on the magnetic interactions. The stronger effect is expected to occur when the Peierls temperature is higher and the electronic gap is increased. In the mean field approach [1], these quantities are correlated by

$$2\Delta = 3.52 k_B T_{CDW}. \tag{6}$$

Nevertheless, one should not underestimate the role played by the Fermi surface nesting vectors. As established from both theoretical predictions [51–55] and experimental results [56–58], in the case of a nontrivial topology of the Fermi surface, the RKKY interaction becomes sensitive to the delicate character of the nesting conditions. The direct link with the FS curvature makes the RKKY interaction strongly anisotropic and leads to the deviations from the simplistic isotropic approach expressed by Eq. (3). The common aspect of the FS nesting and momentum-dependent RKKY interaction lies in the fact that both phenomena are associated with the generalized electron (spin) susceptibility represented by the Lindhard function[51,52,55]:

$$\chi^0(q) \sim \sum_k \frac{f_{k+q} - f_k}{\epsilon_{k+q} - \epsilon_k}, \tag{7}$$

where f_k is the Fermi distribution function and ϵ_k denotes for the energy corresponding to the state with wave vector k. The course, or more strictly, the maximum or a singularity of $\chi^0(q)$ leading to the nesting of the Fermi surface can significantly enhance the strength of the indirect interaction between the magnetic moments. Simultaneously the Fermi surface nesting is a common feature associated with the formation of charge density waves [1,59]. The same Lindhard function determines the energy gain from the electronic part of the CDW. Thus, this function often plays a decisive role for the preferred q vector of the CDW modulation [60], which in most CDW systems is identical with the FS nesting vector. The anisotropic RKKY interaction is therefore significantly enhanced in the specific reciprocal space directions, when the magnetic propagation vector coincides with the values of q corresponding to the maximum of $\chi^0(q)$, consistent with the CDW modulation. The experimental evidence for such nesting enhanced behavior has been reported for Gd_2PdSi_3, Tb_2PdSi_3 [56], GdSi [58], Yttrium [61], or Gd-Y alloys [62]. The CDW modulation vectors for $NdNiC_2$ and $GdNiC_2$ defined from x-ray diffuse scattering experiment, respectively, q_{Nd} = (0.5, 0.52, 0) [41] and q_{Gd} = (0.5, 0.5, 0) [46] have also been theoretically predicted as genuine FS nesting vectors [31]. These vectors stand in agreement with the wave vectors describing the AFM order (0.5, 0.5, 0) observed for $NdNiC_2$ [49,63] and proposed for $GdNiC_2$ [48]. It is reasonable to assume that this coincidence is relevant also for the solid solutions between $NdNiC_2$ and $GdNiC_2$, giving rise to an enhancement of the AFM order due to a cooperative effect with FS nesting accompanying the Peierls instability. The scenario of affirmative coupling between the CDW and magnetism in these systems is also supported by the recent work of Hanasaki *et al.* [43], who

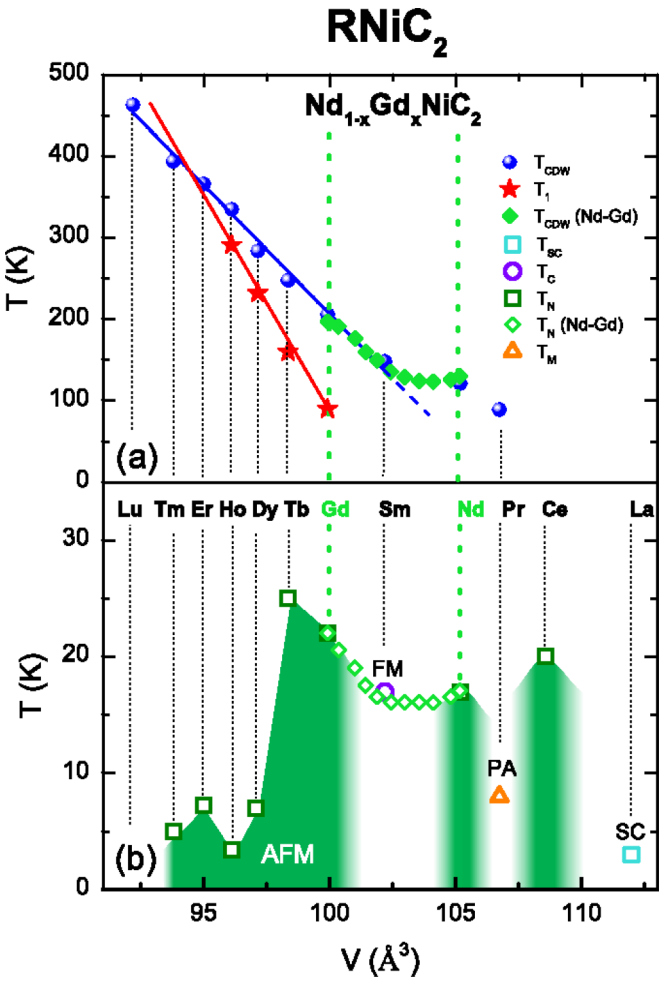

FIG. 7. Phase diagram of the $RNiC_2$ family including $Nd_{1-x}Gd_xNiC_2$ ($0 \leqslant x \leqslant 1$) solid solution. (a) Shows the variation of the Peierls (T_{CDW}) and lock-in (T_1) temperatures with the unit cell volume [[22,26,27,29,30,35,36,46]. (b) Depicts the magnetic ground states with their characteristic temperatures: T_N (Néel), T_C (Curie), and T_M for the paramagnetic anomaly (PA) observed in $PrNiC_2$. T_{SC} marks the onset of superconductivity for $LaNiC_2$.

suggested that the origin of the antiferromagnetic ground state in $GdNiC_2$ lies in the spin density wave constructed upon the preexisting CDW. In this model, the charge density modulated as a result of the Peierls instability is composed of two distinct spin-up and spin-down charge distributions and while the presence of strong magnetic moments produces a phase shift between them, the periodical spin density modulation is formed, giving rise to the enhancement of antiferromagnetic coupling between local f moments.

The values of T_{CDW} and T_N determined in this work have been imposed on the phase diagram of the $RNiC_2$ family, shown in Fig. 7 as a bright green region. It cannot escape from the viewer's eye that these results converge with the trend line $T_{CDW}(V)$ and $T_N(V)$ for $RNiC_2$. It is visible that near the point corresponding to $SmNiC_2$, the charge density wave temperature scaling starts to deviate from linearity. Our results (see Fig. 3) reveal the AFM ground state of all the studied compounds from the $Nd_{1-x}Gd_xNiC_2$ series, even those in a close proximity to $SmNiC_2$, which is a ferromagnet. To confirm the genuine AFM character of the magnetic transitions of the $Nd_{1-x}Gd_xNiC_2$ series, we have measured the M vs H (not shown here) indicating that no ferromagnetic ground state exists below T_N. Additionally, in contrast to $SmNiC_2$ which shows a rapid drop in resistivity below the magnetic transition temperature due to complete destruction of CDW and release of the electronic carriers [37–39], a less abrupt decrease of the $\rho(T)$ curve is seen for $Nd_{1-x}Gd_xNiC_2$ series. The behavior of the solid solutions is reminiscent of the features reported for parent Nd and Gd bearing compounds. In $NdNiC_2$ and $GdNiC_2$, the CDW state partially survives the AFM transition and the similarity between the parent compounds and their solid solution suggests the identity of the observed mechanisms.

IV. CONCLUSIONS

In this article we have examined the transport and magnetic properties of the $Nd_{1-x}Gd_xNiC_2$ ($0 \leqslant x \leqslant 1$) solid solution to explore the evolution of charge density wave and magnetism through the crossover from $NdNiC_2$ towards $GdNiC_2$. The variation of the Peierls temperature of $Nd_{1-x}Gd_xNiC_2$ as a function of the unit cell volume covers suitably the deviation from the linear trend observed in the previous study. We also report the breakdown of the de Gennes scaling in the studied series. The results are discussed in terms of the electric crystal field and indirect Ruderman-Kittel-Kasuya-Yosida interaction between local magnetic moments. The correlation between the Peierls, Néel, and Curie-Weiss temperatures suggests a strong coupling between the Fermi surface nesting and the antiferromagnetic ground state, described by the compatible wave vectors. We also suggest that this hypothesis can be confirmed by the angle-resolved photoemission spectroscopy (ARPES) experiment performed on single crystals.

ACKNOWLEDGMENT

Authors gratefully acknowledge the financial support from National Science Centre (Poland), Grant No. UMO-2015/19/B/ST3/03127.

[1] P. Monceau, Adv. Phys. **61**, 325 (2012).
[2] G. Grüner, *Density Waves in Solids* (Addison-Wesley, Perseus Books Group, Boston, 2000).
[3] G. Grüner, Rev. Mod. Phys. **60**, 1129 (1988).
[4] N. Doiron-Leyraud, S. Lepault, O. Cyr-Choinière, B. Vignolle, G. Grissonnanche, F. Laliberté, J. Chang, N. Barišić, M. K. Chan, L. Ji, X. Zhao, Y. Li, M. Greven, C. Proust, and L. Taillefer, Phys. Rev. X **3**, 021019 (2013).
[5] S. Caprara, C. Di Castro, G. Seibold, and M. Grilli, Phys. Rev. B **95**, 224511 (2017).
[6] V. Thampy, X. M. Chen, Y. Cao, C. Mazzoli, A. M. Barbour, W. Hu, H. Miao, G. Fabbris, R. D. Zhong, G. D. Gu, J. M.

Tranquada, I. K. Robinson, S. B. Wilkins, and M. P. M. Dean, Phys. Rev. B **95**, 241111 (2017).
[7] R. Zhou, M. Hirata, T. Wu, I. Vinograd, H. Mayaffre, S. Krämer, A. P. Reyes, P. L. Kuhns, R. Liang, W. N. Hardy, D. A. Bonn, and M.-H. Julien, Proc. Natl. Acad. Sci. USA **114**, 13148 (2017).
[8] Y. Caplan and D. Orgad, Phys. Rev. Lett. **119**, 107002 (2017).
[9] S. Kawasaki, Z. Li, M. Kitahashi, C. T. Lin, P. L. Kuhns, A. P. Reyes, and G.-q. Zheng, Nat. Commun. **8**, 1267 (2017).
[10] F. Laliberté, M. Frachet, S. Benhabib, B. Borgnic, T. Loew, J. Porras, M. Tacon, B. Keimer, S. Wiedmann, C. Proust, and D. LeBoeuf, npj Quantum Materials **3**, 11 (2018).
[11] O. Cyr-Choinière, R. Daou, F. Laliberté, C. Collignon, S. Badoux, D. LeBoeuf, J. Chang, B. J. Ramshaw, D. A. Bonn, W. N. Hardy, R. Liang, J.-Q. Yan, J.-G. Cheng, J.-S. Zhou, J. B. Goodenough, S. Pyon, T. Takayama, H. Takagi, N. Doiron-Leyraud, and L. Taillefer, Phys. Rev. B **97**, 064502 (2018).
[12] E. Fawcett, Rev. Mod. Phys. **60**, 209 (1988).
[13] V. L. R. Jacques, C. Laulhé, N. Moisan, S. Ravy, and D. Le Bolloc'h, Phys. Rev. Lett. **117**, 156401 (2016).
[14] X. Xu, A. F. Bangura, J. G. Analytis, J. D. Fletcher, M. M. J. French, N. Shannon, J. He, S. Zhang, D. Mandrus, R. Jin, and N. E. Hussey, , Phys. Rev. Lett. **102**, 206602 (2009).
[15] J. Chang, E. Blackburn, A. T. Holmes, N. B. Christensen, J. Larsen, J. Mesot, R. Liang, D. A. Bonn, W. N. Hardy, A. Watenphul, M. v. Zimmermann, E. M. Forgan, and S. M. Hayden, Nat. Phys. **8**, 871 (2012).
[16] J. Chang, E. Blackburn, O. Ivashko, A. T. Holmes, N. B. Christensen, M. Hücker, R. Liang, D. A. Bonn, W. N. Hardy, U. Rütt, M. v. Zimmermann, E. M. Forgan, and S. M. Hayden, Nat. Commun. **7**, 11494 (2016).
[17] D. Graf, E. S. Choi, J. S. Brooks, M. Matos, R. T. Henriques, and M. Almeida, Phys. Rev. Lett. **93**, 076406 (2004).
[18] L. E. Winter, J. S. Brooks, P. Schlottmann, M. Almeida, S. Benjamin, and C. Bourbonnais, Europhys. Lett. **103**, 37008 (2013).
[19] K. Murata, Y. Fukumoto, K. Yokogawa, W. Kang, R. Takaoka, R. Tada, H. Hirayama, J. S. Brooks, D. Graf, H. Yoshino, T. Sasaki, and R. Kato, Physica B: Condensed Matter **460**, 241 (2015).
[20] T. Gruner, D. Jang, Z. Huesges, R. Cardoso-Gil, G. H. Fecher, M. M. Koza, O. Stockert, A. P. Mackenzie, M. Brando, and C. Geibel, Nat. Phys. **13**, 967 (2017).
[21] B. Wiendlocha, R. Szczęśniak, A. P. Durajski, and M. Muras, Phys. Rev. B **94**, 134517 (2016).
[22] W. H. Lee, H. K. Zeng, Y. D. Yao, and Y. Y. Chen, Physica C: Superconductivity **266**, 138 (1996).
[23] V. K. Pecharsky, L. L. Miller, and K. A. Gschneidner, Phys. Rev. B **58**, 497 (1998).
[24] J. Quintanilla, A. D. Hillier, J. F. Annett, and R. Cywinski, Phys. Rev. B **82**, 174511 (2010).
[25] J. F. Landaeta, D. Subero, P. Machado, F. Honda, and I. Bonalde, Phys. Rev. B **96**, 174515 (2017).
[26] H. Onodera, Y. Koshikawa, M. Kosaka, M. Ohashi, H. Yamauchi, and Y. Yamaguchi, J. Magn. Magn. Mater. **182**, 161 (1998).
[27] K. K. Kolincio, M. Roman, M. J. Winiarski, J. Strychalska-Nowak, and T. Klimczuk, Phys. Rev. B **95**, 235156 (2017).
[28] H. Onodera, M. Ohashi, H. Amanai, S. Matsuo, H. Yamauchi, Y. Yamaguchi, S. Funahashi, and Y. Morii, J. Magn. Magn. Mater. **149**, 287 (1995).
[29] P. Kotsanidis, J. Yakinthos, and E. Gamari-Seale, J. Less-Common Met. **152**, 287 (1989).
[30] M. Murase, A. Tobo, H. Onodera, Y. Hirano, T. Hosaka, S. Shimomura, and N. Wakabayashi, J. Phys. Soc. Jpn. **73**, 2790 (2004).
[31] J. Laverock, T. D. Haynes, C. Utfeld, and S. B. Dugdale, Phys. Rev. B **80**, 125111 (2009).
[32] A. Wölfel, L. Li, S. Shimomura, H. Onodera, and S. van Smaalen, Phys. Rev. B **82**, 054120 (2010).
[33] T. Sato, S. Souma, K. Nakayama, T. Takahashi, S. Shimomura, and H. Onodera, J. Phys. Soc. Jpn. **79**, 044707 (2010).
[34] D. Ahmad, B. H. Min, G. I. Min, S.-I. Kimura, J. Seo, and Y. S. Kwon, Phys. Status Solidi B **252**, 2662 (2015).
[35] H. Michor, S. Steiner, A. Schumer, M. Hembara, V. Levytskyy, V. Babizhetskyy, and B. Kotur, J. Magn. Magn. Mater. **441**, 69 (2017).
[36] M. Roman, J. Strychalska-Nowak, T. Klimczuk, and K. K. Kolincio, Phys. Rev. B **97**, 041103 (2018).
[37] S. Shimomura, C. Hayashi, G. Asaka, N. Wakabayashi, M. Mizumaki, and H. Onodera, Phys. Rev. Lett. **102**, 076404 (2009).
[38] N. Hanasaki, Y. Nogami, M. Kakinuma, S. Shimomura, M. Kosaka, and H. Onodera, Phys. Rev. B **85**, 092402 (2012).
[39] H. Lei, K. Wang, and C. Petrovic, J. Phys.: Condens. Matter **29**, 075602 (2017).
[40] J. H. Kim, J.-S. Rhyee, and Y. S. Kwon, Phys. Rev. B **86**, 235101 (2012).
[41] N. Yamamoto, R. Kondo, H. Maeda, and Y. Nogami, J. Phys. Soc. Jpn. **82**, 123701 (2013).
[42] K. K. Kolincio, K. Górnicka, M. J. Winiarski, J. Strychalska-Nowak, and T. Klimczuk, Phys. Rev. B **94**, 195149 (2016).
[43] N. Hanasaki, S. Shimomura, K. Mikami, Y. Nogami, H. Nakao, and H. Onodera, Phys. Rev. B **95**, 085103 (2017).
[44] J. Rodríguez-Carvajal, Physica B: Condensed Matter **192**, 55 (1993).
[45] W. Jeitschko and M. H. Gerss, J. Less-Common Met. **116**, 147 (1986).
[46] S. Shimomura, C. Hayashi, N. Hanasaki, K. Ohnuma, Y. Kobayashi, H. Nakao, M. Mizumaki, and H. Onodera, Phys. Rev. B **93**, 165108 (2016).
[47] N. Hanasaki, K. Mikami, S. Torigoe, Y. Nogami, S. Shimomura, M. Kosaka, and H. Onodera, J. Phys.: Conf. Ser. **320**, 012072 (2011).
[48] S. Matsuo, H. Onodera, M. Kosaka, H. Kobayashi, M. Ohashi, H. Yamauchi, and Y. Yamaguchi, J. Magn. Magn. Mater. **161**, 255 (1996).
[49] J. Yakinthos, P. Kotsanidis, W. Schäfer, and G. Will, J. Magn. Magn. Mater. **89**, 299 (1990).
[50] Y. Koshikawa, H. Onodera, M. Kosaka, H. Yamauchi, M. Ohashi, and Y. Yamaguchi, J. Magn. Magn. Mater. **173**, 72 (1997).
[51] L. M. Roth, H. J. Zeiger, and T. A. Kaplan, Phys. Rev. **149**, 519 (1966).
[52] P. Bruno and C. Chappert, Phys. Rev. B **46**, 261 (1992).
[53] D. N. Aristov and S. V. Maleyev, Phys. Rev. B **56**, 8841 (1997).
[54] D. N. Aristov and S. V. Maleyev, Physica B: Condensed Matter **284-288**, 1351 (2000).
[55] E. Simon, B. Lazarovits, L. Szunyogh, and B. Újfalussy, Philos. Mag. **88**, 2667 (2008).
[56] D. S. Inosov, D. V. Evtushinsky, A. Koitzsch, V. B. Zabolotnyy, S. V. Borisenko, A. A. Kordyuk, M. Frontzek, M. Loewenhaupt, W. Löser, I. Mazilu, H. Bitterlich, G. Behr, J.-U. Hoffmann, R. Follath, and B. Büchner, Phys. Rev. Lett. **102**, 046401 (2009).

[57] L. Zhou, J. Wiebe, S. Lounis, E. Vedmedenko, F. Meier, S. Blügel, P. H. Dederichs, and R. Wiesendanger, Nat. Phys. **6**, 187 (2010).
[58] Y. Feng, J. Wang, D. M. Silevitch, B. Mihaila, J. W. Kim, J.-Q. Yan, R. K. Schulze, N. Woo, A. Palmer, Y. Ren, J. v. Wezel, P. B. Littlewood, and T. F. Rosenbaum, Proc. Natl. Acad. Sci. USA **110**, 3287 (2013).
[59] M. D. Johannes and I. I. Mazin, Phys. Rev. B **77**, 165135 (2008).
[60] K. Rossnagel, J. Phys.: Condens. Matter **23**, 213001 (2011).
[61] S. B. Dugdale, H. M. Fretwell, M. A. Alam, G. Kontrym-Sznajd, R. N. West, and S. Badrzadeh, Phys. Rev. Lett. **79**, 941 (1997).
[62] H. M. Fretwell, S. B. Dugdale, M. A. Alam, D. C. R. Hedley, A. Rodriguez-Gonzalez, and S. B. Palmer, Phys. Rev. Lett. **82**, 3867 (1999).
[63] W. Schäfer, G. Will, J. Yakinthos, and P. Kotsanidis, J. Alloys Compd. **180**, 251 (1992).